I&EC research
Industrial & Engineering Chemistry Research

pubs.acs.org/IECR

Article

A First-Principles Approach for Control-Oriented Modeling of De-oiling Hydrocyclones

Mishiga Vallabhan K G,* Christian Holden,* and Sigurd Skogestad*

Cite This: *Ind. Eng. Chem. Res.* 2020, 59, 18937−18950

Read Online

ACCESS | Metrics & More | Article Recommendations

ABSTRACT: De-oiling hydrocyclones are a promising choice for produced water treatment in the oil and gas industry. The compact nature of hydrocyclones makes them suitable for offshore and subsea installations. The commitment toward reduction in environmental footprint makes it a necessity to maintain the efficiency of the produced water treatment system (hydrocyclones) under all plant scenarios. A mathematical model for de-oiling hydrocyclones can help to develop robust control algorithms to handle the uncertainties and to maintain high efficiency. In this paper, a simple first-principle model is developed for hydrocyclones. A pressure-flow relationship is derived using Bernoulli's equation, a droplet trajectory analysis is done for calculating the separation, and a dynamic mass balance is used for control purposes. A simple PI control algorithm tuned using the SIMC tuning rules is used to verify the model and its control properties.

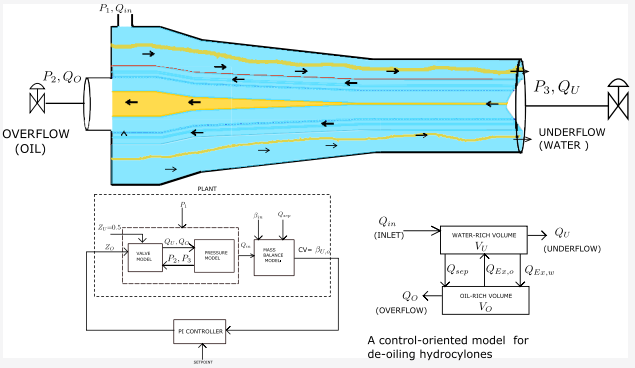

INTRODUCTION

Produced water is a common waste product in oil and gas production. The amount of produced water typically increases with the age of the oil field. Two common methods for produced water treatment are reinjection into the reservoir and discharge to the sea. Reinjection of produced water increases the reservoir pressure and hence may enhance recovery. Discharge of produced water to sea has to meet local governmental regulations. The Norwegian continental shelf comes under the regulation of the OSPAR commission, which has set a limit of 30 mg/L of oil (approximately 30 ppm) in produced water discharged to the sea.[1] Hydrocyclones, compact floatation units (CFUs), and membrane filters are equipment used for produced water treatment.

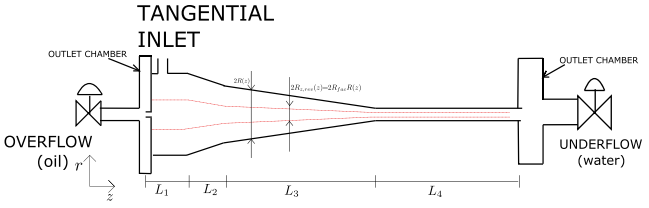

Figure 1. Hydrocyclone liner connected to two outlet chambers (not drawn to scale). The red lines represent the reverse-flow zone.

Almost 90% of the offshore produced water treatment facilities are based on hydrocyclone technology.[2] Simple, lightweight, compact nature of hydrocyclones along with low maintenance costs makes it attractive for the subsea environment as well. The Brazilian Marlim field at 870 m water depth has subsea oil−water separation with a hydrocyclone for produced water treatment.[3,4] This is the only one currently in use subsea.

Since the 1800s, hydrocyclones have been the most popular separation technology in the mining and mineral industry.[5] Later, the oil and drilling industry used simple and rugged cyclone devices for sand separation from oil, drilling mud, and other fluids. In the 1970s, trials began on the possibility of using hydrocyclones to separate oil−water mixtures. By modifying certain geometry and design parameters, the conventional hydrocyclones achieved adequate separation of oil−water mixtures.

The first experimental results were given in ref 6, and in that paper, it is mentioned that the efficiency of cyclones largely depends on the oil droplet size. Design guidelines and advantages and disadvantages of de-oiling hydrocyclones used in offshore platforms are given in ref 7. Details about the

Received: June 8, 2020
Revised: September 23, 2020
Accepted: September 25, 2020
Published: September 25, 2020

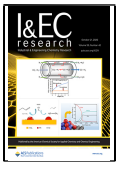

construction and principle of operation of the first full-scale commercial de-oiling hydrocyclone are given in ref 8. Reference 9 gives details about factors such as separation efficiency, feed characteristics (inflow rate, oil water ratio, etc.), pressure drop, and operation.

There are two different types of de-oiling hydrocyclones: one has a swirl element inside the cyclone (called inline hydrocyclones), whereas the one studied in this paper is without a swirl element. A control-oriented modeling of an inline hydrocyclone is given by ref 10.

This paper focuses on hydrocyclones without a swirl element as shown in Figure 1. The geometry itself induces swirling in these types of cyclones. There have been numerous studies on modeling of de-oiling hydrocyclones without a swirl element. A model to calculate the efficiency of liquid−liquid hydrocyclones based on droplet trajectories is presented in ref 11, where the three velocity components (tangential, axial, and radial) are used for trajectory analysis. Later, ref 12 developed a mechanistic model for liquid−liquid hydrocyclones where the separation efficiency is determined based on swirl intensity and droplet trajectory analysis. They also present a model to predict the pressure drop from the inlet to the underflow outlet. Most recently, CFD-based studies on the velocity distribution and separation performance have become popular, for example, refs 13 and 14.

Most of the models developed for de-oiling hydrocyclones, for example, CFD models, are too complicated and not suitable from a control perspective. One approach for control-oriented modeling of a hydrocyclone is given in ref 15, where experimental data was used to derive transfer function models. Later, ref 16 developed a gray-box model based on flow resistance and droplet trajectory analysis for determining the separation efficiency of hydrocyclones. However, more simple first principles-based models have not been investigated. In this paper, a control-oriented model for a hydrocyclone is derived by combining droplet trajectory analysis, pressure-flow relationships, and a dynamic mass-balance model.

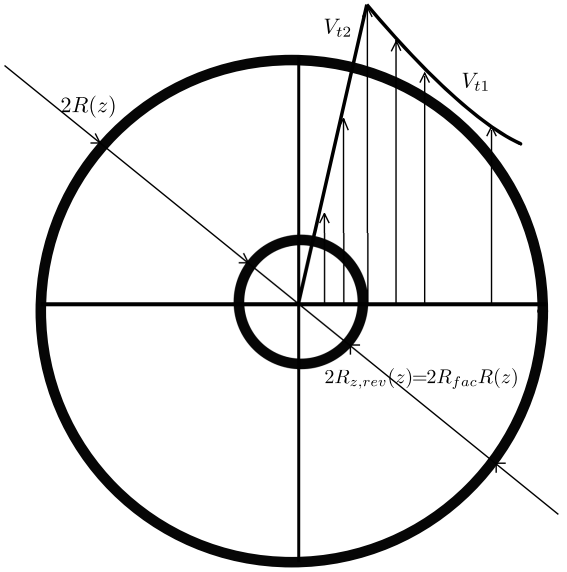

Figure 2. Tangential velocity profile inside a hydrocyclone liner.

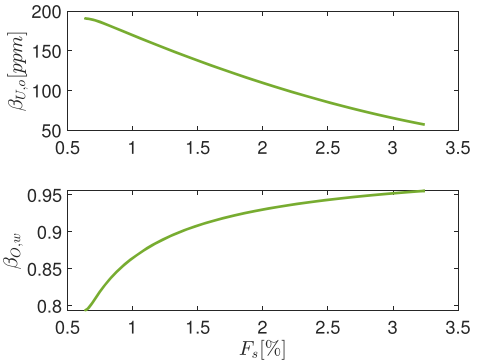

Figure 3. Variation of oil in underflow and water in overflow with flow split. The figure was obtained using the model presented later in this paper (here $\beta_{in,\,o}$=1500 ppm).

HYDROCYCLONE MODELING: INTRODUCTION

De-oiling hydrocyclones have a cluster of cyclone liners, which can be added or removed in order to meet flow rate requirements. Each liner has a tangential inlet and two outlets (see Figure 1). The heavy purified water comes out through the underflow outlet, and the lighter oil-rich stream comes out through the overflow outlet. The outflows from all of the liners enter into the two outlet chambers at the overflow and underflow ends. Figure 1 shows a single liner connected to two outlet chambers.

A hydrocyclone liner has four sections: first, a cylindrical part where the liquid enters; second, a tapered conical section where the fluid is accelerated due to the reduction in the diameter; third, a longer tapered conical section where the majority of the separation occurs; and fourth, a parallel tail section where slower-moving droplets can be recovered.

Separation occurs due to centrifugal forces, which are much larger in magnitude than the ones in a conventional gravity-based separator.[8] The tangential inlet section aids in generating the centrifugal force, and the narrowing section of hydrocyclones further accelerates the fluid. The low-density oil droplets move toward the center of the cyclone and form the reverse oil core, which exits at the overflow outlet. At the same time, the higher-density water is pushed toward the walls of the cyclone and carried away as the continuous phase to the underflow outlet.

There exists a reverse-flow zone inside a hydrocyclone liner. The oil droplets entering the reverse-flow zone get separated from the continuous phase and form an oil-rich reverse core at the center of the cyclone liner.

According to ref 12, the location of the reverse-flow zone depends on the swirl intensity. Thus, it is a function of cyclone geometry, the mean axial velocity, and the tangential velocity. In ref 11, the reverse-flow zone is calculated based on the axial velocity profile, which varies with the sections of the hydrocyclone. Hence, we can say that depending on the sections L_1 to L_4 (in Figure 1), the size of the reverse-flow zone varies. Also, while, the reverse-flow zone extends to the underflow,[7] oil present in the reverse-flow zone does not go out through the underflow outlet:

$$R_{z,rev}(z) = R_{fac}(z)R(z) \tag{1}$$

where $R(z)$ is the radius of hydrocyclone at different axial positions z. From refs 12 and 11 , we can say the factor R_{fac} has four different values at four sections L_1, L_2, L_3, and L_4. As the separation mainly takes place in L_3 and L_4, we assume two values for R_{fac}, i.e., $R_{fac,1}$ when it is in sections L_1 to L_3 and $R_{fac,2}$ when it is

https://dx.doi.org/10.1021/acs.iecr.0c02859
Ind. Eng. Chem. Res. 2020, 59, 18937−18950

in L_4 where $1 > R_{fac,1} > R_{fac,2}$. $R_{fac,1}$ and $R_{fac,2}$ are tuning parameters in the model, and we will use values of 0.3714 and 0.27.

The flow pattern inside a hydrocyclone can be described using three velocity components: tangential (θ), axial (z), and radial (r). The tangential velocity shows a Rankine vortex-type rotational behavior as shown in Figure 2.[11] Starting from the hydrocyclone wall, the velocity increases and reaches a maximum. The point where the tangential velocity reaches its maximum is the starting point of the reverse-flow zone for the axial velocity.[12] This is called a locus of zero axial velocity. Further away from this point, the tangential velocity starts to decrease and it approaches zero at the center of the hydrocyclone. The radial velocity distribution depends on the Stokes drag.

A hydrocyclone separates inlet feed into two products, so there are two operational quantities of interest: the fraction of oil in the underflow (water reject), $\beta_{U,o}$ (which is our main concern), and the fraction of water in the overflow (oil reject), $\beta_{O,w}$. Reference 7 defines the separation in terms of two parameters. One is the separation efficiency, defined as

$$\eta = 1 - \frac{\beta_{U,o}}{\beta_{\text{in},o}} \tag{2}$$

where $\beta_{U,o}$ and $\beta_{in,o}$ are the fraction of oil in the underflow and the inlet, respectively. Here, the subscript o denotes oil, U denotes underflow, and O denotes overflow.

The second parameter is the flow split, defined as

$$F_s = \frac{Q_O}{Q_{\text{in}}} \tag{3}$$

where Q_O is overflow rate and Q_{in} is the inflow rate. A high-performing hydrocyclone should have a high separation efficiency and a small flow split. However, there is a trade-off between the two parameters. This is seen from Figure 3, where we see that to reduce $\beta_{U,o}$ to get a high separation efficiency (desired), we need to increase the flow spilt (F_s) (undesired). From the lower plot, we see that an increase in the flow spilt also increases the fraction of water in the overflow. We also see that the overflow ("oil") contains mostly water, about 80−95% in this case.

In this paper, the hydrocyclone modeling is focused on the control aspects. The flow between the inlet and the two outlets is modeled based on Bernoulli's equation assuming laminar flow (Pressure-Flow Relationship section). The separation and separation efficiency are calculated based on a droplet trajectory model (Oil Droplet Trajectory Analysis and Modeling of Internal Separation sections). The flow and droplet trajectory models are steady-state in nature. Dynamics, which may be required for control purposes, are incorporated in the mass balances by dividing the hydrocyclone into two main control volumes (Dynamic Mass-Balance Model section).

PRESSURE-FLOW RELATIONSHIP

This section derives a static relationship between pressures (P_1, P_2, P_3) and volumetric flow rates (Q_U, Q_O) (marked in Figure 4a) assuming:

A1. The size of the reverse-flow zone is fixed, and the reverse-flow zone extends through the length of the hydrocyclone. In other words, a Rankine vortex flow pattern exists from the inlet to the underflow.

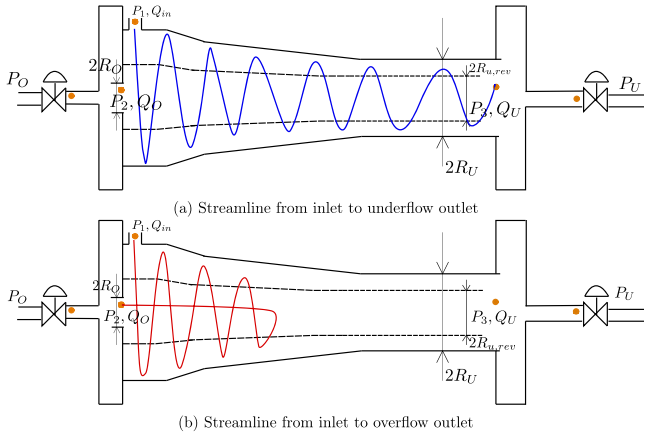

Figure 4. Different streamline considered for calculating the pressure-flow relationship of a hydrocyclone.

Table 1. Parameters Used for Simulation

parameter	value	unit
P_1	6	bar
P_{atm}	1.01325	bar
ρ_O	910	kg/m^3
$\rho_U = \rho_w$	1000	kg/m^3
ρ	989	kg/m^3
R_{in}	0.0035	m
R_O	0.001	m
R_U	0.005	m
V_{HC}	2.0896×10^{-04}	m^3
V_O	5.2239×10^{-07}	m^3
C_D	20	
C_{v1}	5.0671×10^{-05}	m^2
C_{v2}	2.5335×10^{-06}	m^2

A2. The radial velocities at the exit points are negligible.

A3. The frictional losses inside the cyclones are neglected in Bernoulli's equation.

First, consider a water streamline between a point at the tangential inlet and a point at the underflow. This is marked in blue in Figure 4a. Then, from Bernoulli's equation, with no friction loss (Assumption A3), we get:

$$P_1 + \frac{\rho}{2}\left(\frac{Q_{\text{in}}}{A_{\text{in}}}\right)^2 = P_3 + \text{KE}_{\text{Uz}} + \text{KE}_{U\theta}$$

Here, KE_{Uz} is the kinetic energy contributed by the axial velocity of the fluid we have

$$\text{KE}_{\text{Uz}} = \frac{\rho_U}{2}\left(\frac{Q_U}{A_U}\right)^2$$

where A_U is the underflow cross-sectional area and Q_U is the underflow volumetric flow rate. The kinetic energy contributed by the tangential velocity is given $\text{KE}_{U\theta}$. The tangential velocity profile at the underflow is a combination of free and forced vortexes. The detailed derivation of the $\text{KE}_{U\theta}$ is given in Appendix A. Inserting into Bernoulli's equation gives

$$P_1 + \frac{\rho}{2}\left(\frac{Q_{\text{in}}}{A_{\text{in}}}\right)^2 = P_3 + \frac{\rho_U}{2}\left(\frac{Q_U}{A_U}\right)^2 + \frac{5}{4}\frac{\rho_U}{R_U^2}\frac{(\alpha_1 Q_{\text{in}} R_1)^2}{\pi^2 R_{\text{in}}^4} \tag{4}$$

https://dx.doi.org/10.1021/acs.iecr.0c02859
Ind. Eng. Chem. Res. 2020, 59, 18937−18950

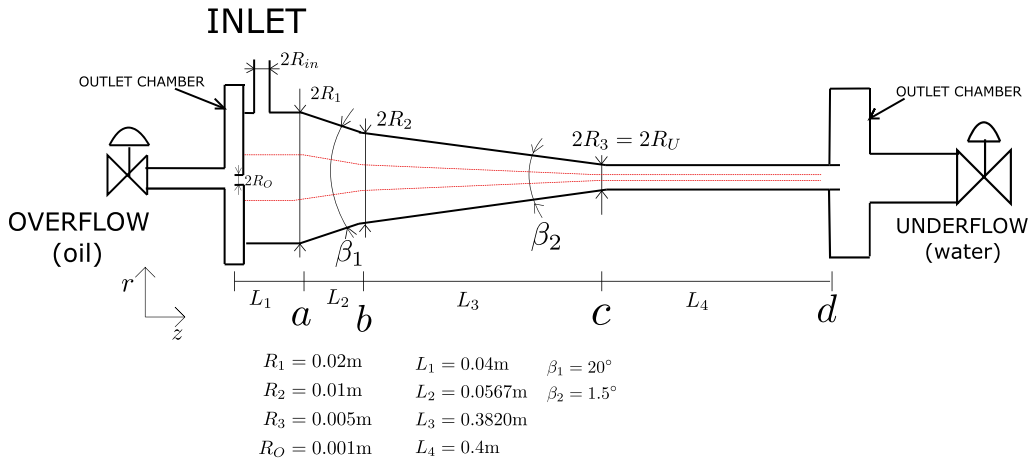

Figure 5. Geometrical details of a hydrocyclone liner used in the model (not drawn to scale).

Next, a second oil streamline is considered between a point at the tangential inlet and a point at the overflow as shown by a red line in Figure 4b. From Bernoulli's equation and Assumption A3, we get

$$P_1 + \frac{\rho}{2}\left(\frac{Q_{in}}{A_{in}}\right)^2 = P_2 + KE_{Oz} + KE_{O\theta}$$

where the kinetic energy in the axial direction is

$$KE_{Oz} = \frac{\rho_O}{2}\left(\frac{Q_O}{A_O}\right)^2$$

The tangential velocity profile at the overflow has only forced vortex, and hence the forced velocity component contributes to the kinetic energy $KE_{O\theta}$. The detailed derivation for this term is given in Appendix B. The Bernoulli's equation can then be rewritten as

$$P_1 + \frac{\rho}{2}\left(\frac{Q_{in}}{A_{in}}\right)^2 = P_2 + \frac{\rho_O}{2}\left(\frac{Q_O}{A_O}\right)^2 + \frac{\rho_O}{4}\frac{(\alpha_1 Q_{in} R_1)^2}{(\pi R_{in}^2)^2 R_{U,rev}^4} R_O^2 \quad (5)$$

Next, consider the pressure at two exits of the liner, thus can be modeled using a standard valve equation for turbulent flow. This gives

$$Q_U = C_{v1} Z_U \sqrt{\frac{2(P_3 - P_U)}{\rho_U}} \quad (6)$$

$$Q_O = C_{v2} Z_O \sqrt{\frac{2(P_2 - P_O)}{\rho_O}} \quad (7)$$

Here, C_{v1} and C_{v2} are the valve constants of the underflow and overflow valves (incorporating frictional losses), P_2 is the pressure at the overflow outlet, P_3 is the pressure at the underflow outlet, $Z_U \in [0,1]$ and $Z_O \in [0,1]$ are the valve positions, and ρ_U and ρ_O are the densities of liquid at the underflow and overflow outlets, respectively. P_O is the downstream pressure of the overflow valve, and P_U is the downstream pressure of the underflow valve . This paper assumes that P_O and P_U are known and equal to the atmospheric pressure (P_{atm}).

Finally, from the overall mass balance:

$$Q_{in} = Q_O + Q_U \quad (8)$$

In the five (eqs 4−8), there are six unknowns (Q_{in}, P_1, Q_O, P_2, Q_U, P_3). TThen, either the inlet flow Q_{in} or the inlet pressure P_1 is assumed as a known boundary condition and the other unknowns can be found by solving the equations.

As an example, consider that we know P_1 = 600 kPa and the valve positions are $Z_U = Z_O = 0.4$. Then with data in Table 1, we get, P_2 = 470 kPa, P_3 = 539 kPa, $\frac{\rho}{2}\left(\frac{Q_{in}}{A_{in}}\right)^2$ = 132 kPa, $Q_O = 2.88 \times -5$ m^3/s, $Q_U = 5.99 \times 10^{-4}$ m^3/s, KE_{Uz} = 29 kPa, $KE_{U\theta}$ = 163 kPa, KE_{Oz} = 38 kPa, and $KE_{O\theta}$ = 224 kPa.

OIL DROPLET TRAJECTORY ANALYSIS

The separation efficiency of the hydrocyclone depends on the centrifugal force acting on the two fluid components (oil and water) and the frictional (drag) force acting on the dispersed oil particles. We divide our analysis into two parts: continuous phase (water) and dispersed oil phase. Two simplifying assumptions for this analysis are as follows:

A4. Axisymmetric flow.

A5. The tangential velocity is not zero at the walls.

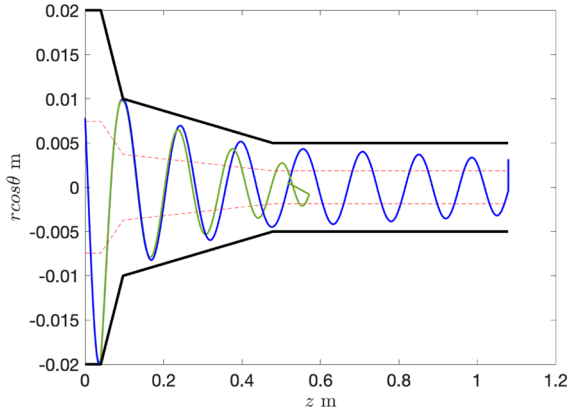

Figure 6. Simulated trajectory of 50 μm oil droplet (green), which is separated as its enters the reverse-flow zone (marked in red), and 5 μm (blue), which is not separated and comes out as underflow. The black marking represents the walls of the hydrocyclone. The picture shows a two-dimensional view of the simulation, and this is why the green line does not reverse immediately when it crosses the red line.

https://dx.doi.org/10.1021/acs.iecr.0c02859
Ind. Eng. Chem. Res. 2020, 59, 18937−18950

Continuous Phase (Water). The three velocity components of the continuous water phase are the tangential velocity $v_{\theta,w}$, the axial velocity $v_{z,w}$, and the radial velocity $v_{r,w}$. Here, the subscript w denotes the water phase, whereas we will use o to denote the oil phase.

Tangential Velocity. The tangential velocity profile inside the hydrocyclone exhibits a Rankine vortex-type behavior (as shown in Figure 2), where the free vortex occurs near the cyclone wall and the forced vortex occurs near the axis of the hydrocyclone.[11,12] Hence, the tangential velocity is a function of radial position; the velocity decreases as the radial position increases in the free-vortex region, and in the forced-vortex region, the velocity increases as the radial position increases. Then, based on the conservation of angular momentum, the following expression holds for the tangential velocity:

$$v_{\theta,w}(r)r^n = \text{constant}$$

Here, $v_{\theta,w}(r)$ is the tangential velocity at the radial position r. The value of n varies between -1 (forced vortex) and 1 (free vortex). As most of the separation takes place near the semi-free vortex region,[11] we will for simplicity use one value for n, in the region from 0.5 to 0.9.[11] The constant can be found from the known inlet velocity and inlet radius.

A tuning factor $\alpha_1 \leq 1$ is introduced to enable the calculation of the tangential velocity of the fluid at any given radial position based on the inlet velocity v_{in} and the radius of the first cylindrical part of the cyclone R_1 (see Figure 5). Hence, the tangential velocity is given as

$$v_{\theta,w}(r)r^n = \alpha_1 v_{\text{in}} R_1^n = \alpha_1 \frac{Q_{\text{in}}}{A_{\text{in}}} R_1^n \tag{9}$$

Axial Velocity. The axial velocity of the fluid in the low cone section is given as a polynomial approximation in refs 12 and 11. In our paper, the axial velocity of the continuous phase is modeled as a flow through a pipe of changing diameter. A standard flow model for a two-dimensional converging nozzle is[17]

$$v_z(z) = U_0\left(1 + \frac{z}{L}\right) \tag{10}$$

$$v_r(r) = -U_0\frac{r}{L} \tag{11}$$

Here, v_z is the axial velocity, v_r is the radial velocity, L is the length of the converging nozzle, and U_0 is the initial axial velocity. With this simple flow model, the axial velocity profile of a hydrocyclone is given below:

$$v_{z,w}(z) = V_0(z)\left(1 + \frac{z - Z}{L(z)}\right) \tag{12}$$

$$L(z) = \begin{cases} \infty & \text{if } z \leq a \\ L_2 & \text{if } a < z \leq b \\ L_3 & \text{if } b < z \leq c \\ \infty & \text{if } c < z \leq d \end{cases} \tag{13}$$

$$V_0(z) = \begin{cases} V_0 & \text{if } z \leq a \\ V_0 & \text{if } a < z \leq b \\ V_0\left(1 + \frac{(b-a)}{L_2}\right) & \text{if } b < z \leq c \\ V_0\left(1 + \frac{(b-a)}{L_2}\right)\left(1 + \frac{(c-b)}{L_3}\right) & \text{if } c < z \leq d \end{cases} \tag{14}$$

$$Z = \begin{cases} 0 & \text{if } z \leq a \\ a & \text{if } a < z \leq b \\ b & \text{if } b < z \leq c \\ c & \text{if } c < z \leq d \end{cases} \tag{15}$$

$$V_0 = \frac{Q_U}{\pi R_1^2} \tag{16}$$

Here, R_1 is the radius of the first cylindrical part of the hydrocyclone and Q_U is the volumetric flow rate toward the underflow.

The limits used in eqs 13−15 are marked in Figure 5. The axial flow described above is from the inlet to the underflow. However, there is a reverse-flow toward the overflow outlet, and hence the actual axial velocity will be higher than the one described by eq 16 as the total cross-sectional area is slightly smaller. Rewriting the initial velocity after considering the reverse-flow zone with a fixed radius of R_{fac} gives

$$V_0 = \alpha_2 \frac{1}{(1 - R_{fac})^2}\frac{Q_U}{\pi R_1^2} \tag{17}$$

where a tuning parameter $\alpha_2 \geq 1$ has been added to the initial velocity to capture higher tangential velocity at the inlet.

Radial Velocity. From eq 11, the radial velocity of the water is given as

$$v_{r,w}(r, z) = -V_0(z)\left(\frac{r}{L(z)}\right) \tag{18}$$

Dispersed Phase (Oil). The droplet trajectory analysis for the dispersed oil phase is done using the three velocity components $v_{r,o}$, $v_{\theta,o}$, and $v_{z,o}$. The oil tangential velocity $v_{\theta,o}$ and the axial velocity $v_{z,o}$ are assumed to be same as for the continuous water phase, i.e.

$$v_{\theta,o} = v_{\theta,w} \tag{19}$$

$$v_{z,o} = v_{z,w} \tag{20}$$

In the radial direction, the oil drops move relative to the continuous water phase because of the difference in the centrifugal forces, as given by the density difference $\rho_o - \rho_w$. In addition, the oil droplets have a frictional (drag) force acting on them. In our analysis, we consider this to be a quadratic drag as in ref 12. The combined effect of these forces makes the oil droplets achieve a terminal/settling velocity relative to the water phase, given as

$$v_{ter}(r) = \sqrt{\frac{4}{3}\frac{(\rho_o - \rho_w)}{\rho_o}\frac{v_{\theta,w}^2 D}{rC_D}} \tag{21}$$

https://dx.doi.org/10.1021/acs.iecr.0c02859
Ind. Eng. Chem. Res. 2020, 59, 18937−18950

where D is the diameter of oil droplet, r is the radial position of oil droplet, ρ_o is the density of the oil, ρ_w is the density of water, and C_D is the drag coefficient. Then, the total radial velocity of the dispersed oil phase is given as

$$v_{r,o} = v_{r,w} + v_{ter} \tag{22}$$

Numerical values of the hydrocyclone dimensions used in the simulations are given in Figure 5. Figure 6 shows the simulation of droplet trajectories using eqs 19, 20, 21, and 22. The black color marking in the figure represents the physical boundary of a hydrocyclone liner, the red dashed marking represents the reverse-flow zone. Here, average axial velocity $v_{z,o}$ is primarily used for calculating the residence time of the droplets in the forward-flow zone. The radial velocity $v_{r,o}$ is used for checking the droplets reaching the reverse-flow zone.

Oil droplets that enter the reverse-flow zone are considered to be separated from the water, see the green trajectory in Figure 6, which represents a 50 μm droplet. It is not necessary for our approach to calculate the internal separation (Modeling of Internal Separation section) to track the droplets after entering the reverse-flow zone, Hence, the trajectory in the figure stops abruptly after entering the reverse-flow zone. The blue marking in Figure 6 represents a trajectory of a 5 μm droplet, and this droplet is not separated as it is not able to enter the reverse-flow zone.

The simulation of droplet categories from 5 to 60 μm using trajectory models 19, 20, 21, and 22 resulted in separation of oil droplets greater than 10 μm.

MODELLING OF INTERNAL SEPARATION

In this paper, a droplet trajectory analysis is used for calculating the separation inside the cyclone. Using eqs 19−22, if an oil droplet reaches the reverse-flow zone before exiting through the underflow, then it is assumed to be separated. The separated oil moves toward the oil-rich reverse core and comes out as underflow. However, there can also exist situations where the entire oil-rich core gets filled by oil and the overflow opening is not large enough to take it out; and the excess oil has to come out through the underflow outlet. In the Dynamic Mass-Balance Model section, a simple approach to capture this scenario is described.

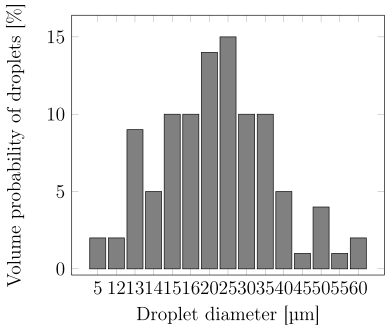

Figure 7. Sample droplet distribution at the inlet of the hydrocyclone.

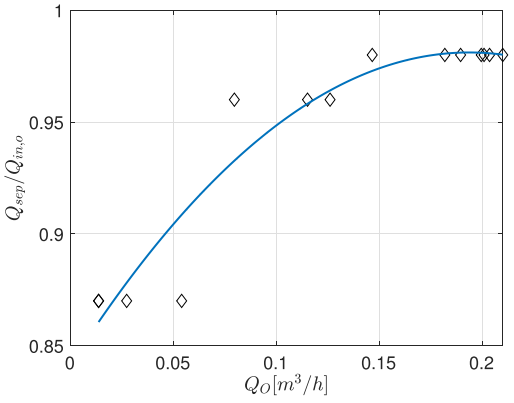

Figure 9. Internal separation $\frac{Q_{sep}}{Q_{in,o}}$ as a function of overflow rate Q_O with fixed underflow valve opening.

The oil droplets at the inlet of a hydrocyclone are assumed to range from 5 to 60 μm.[11,18] We will assume that we know the inlet oil droplet distribution.

It is not feasible to simulate all the droplets entering the cyclone one by one (as there are too many), so we simulate a single droplet from each size category and find where it ends up. If the droplet enters the reverse-flow zone before reaching the end of the cyclone, then we assume that all droplets in that category are separated.

We make the following assumptions:

A6. A mixture with 1000 ppm oil with a droplet distribution as shown in Figure 7 enters the hydrocyclone.

A7. Droplets of 15 different diameters: 5 μm, 12 μm, 13 μm, 14 μm, 15 μm, 16 μm, 20 μm, 25 μm, 30 μm, 35 μm, 40 μm, 45 μm, 50 μm, 55 μm, and 60 μm.

A8. All the droplets have the same starting position, and droplet trajectories are tracked using eqs 19−22.

A9. Droplets reaching the reverse-flow zone are separated.

Summing up the volume fraction of droplet categories entering the reverse-flow zone gives the total fraction of the separated droplets. The separation in the hydrocyclone varies with the inflow rate; this can be either due to the variation in residence time or due to the variation of the drag force acting on the oil droplets. It is clear from eq 17 that the axial velocity is influenced by the inflow rate, and thus if the inflow rate is reduced, then the droplets get more residence time and this

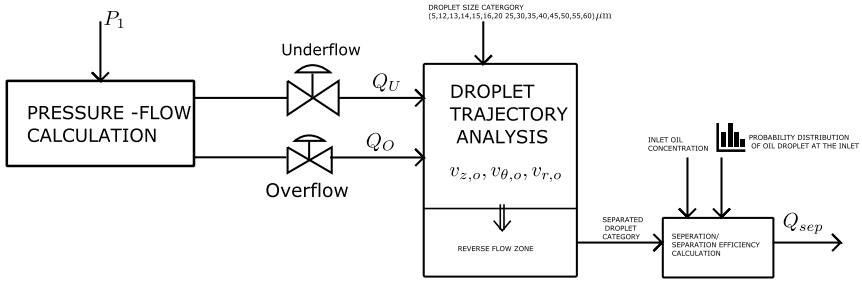

Figure 8. Diagrammatic representation of the calculation of internal separation Q_{sep} (Modeling of Internal Separation section).

https://dx.doi.org/10.1021/acs.iecr.0c02859
Ind. Eng. Chem. Res. 2020, 59, 18937−18950

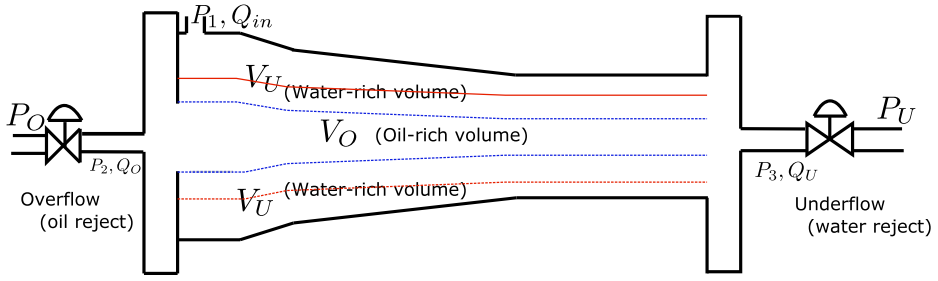

(a) Main zones.

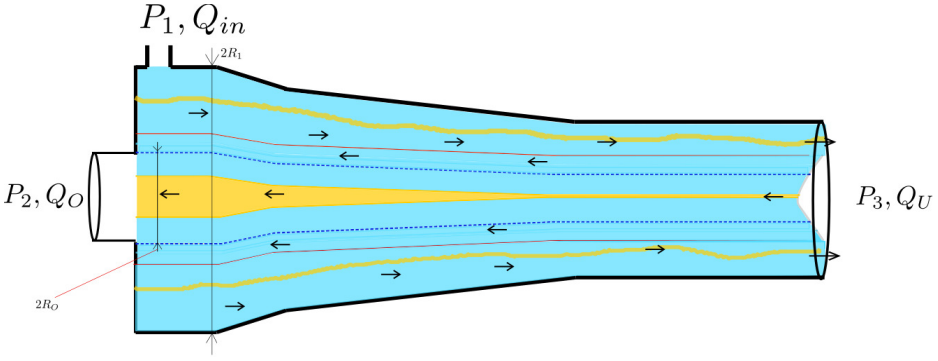

(b) Case with large overflow Q_O causing excess water to enter overflow.

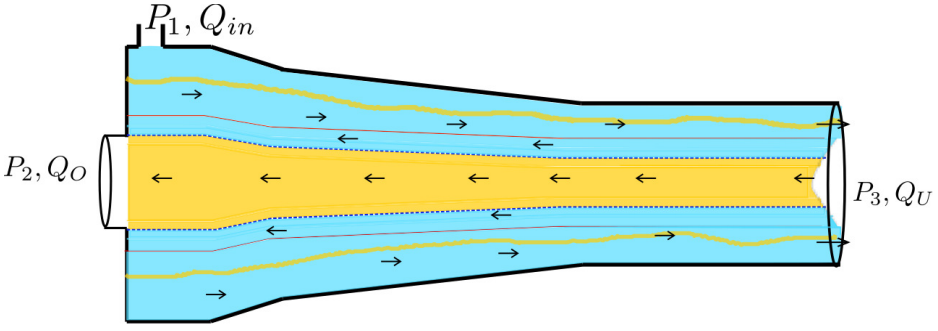

(c) Case with balanced overflow Q_O.

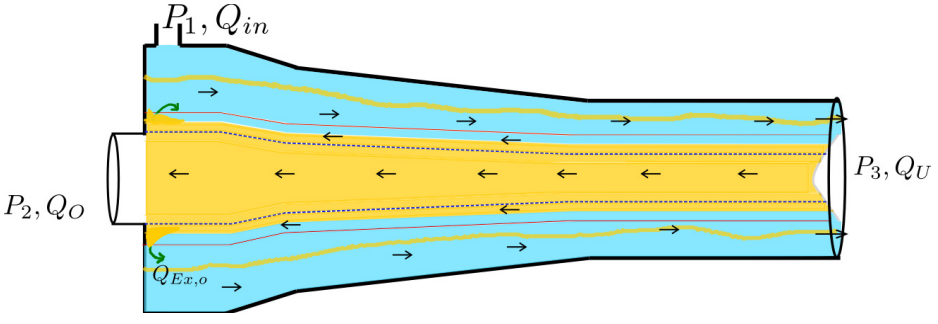

(d) Case when overflow Q_O is too small and excess separated oil returns (green arrows).

Figure 10. Pictorial representation of a hydrocyclone liner. The red lines represent the reverse-flow zone, yellow represents oil, and blue represents water.

increases the separation. However, a decrease in the inflow rate decreases the drag force (from eqs 9 and 22) and this decreases the separation. Hence, these two effects counteract each other, and careful analysis needs to be done based on the region of operation.

The separation can be expressed in terms of volumetric flow as $\frac{Q_{sep}}{Q_{in,o}}$, where Q_{sep} is the volumetric flow rate of the separated oil inside the cyclone and $Q_{in,o}$ is the volumetric flow rate of the incoming oil. According to eq 8, the inflow rate of the cyclone can be varied by either changing the overflow rate or the underflow rate. We can vary the overflow rate Q_O with a fixed underflow valve opening to change the inflow rate and calculate the separation. Figure 8 summarizes the method used for calculating the internal separation. We derive an empirical relationship between the overflow rate and $\frac{Q_{sep}}{Q_{in,o}}$, which can be used in a control-oriented model. We use a second-order polynomial approximation:

https://dx.doi.org/10.1021/acs.iecr.0c02859
Ind. Eng. Chem. Res. 2020, 59, 18937−18950

$$\frac{Q_{sep}}{Q_{\text{in},o}} = p_2 Q_O^2 + p_1 Q_O + p_0 \tag{23}$$

To generate the data, the overflow valve opening is changed from 1% to 100% with inlet pressure P_1 at 6 bar, fixed underflow opening at 40%, inlet oil concentration as 1000 ppm, and the droplet distribution as shown in Figure 7. The resulting data are shown by the diamonds in Figure 9. Here, Q_O = 0.222 m^3/h corresponds to 100% overflow valve opening. A least-squares curve fit gives $p_2 = -4.821 \times 10^7$, p_1 = 5190, and p_0 = 0.8414. Here, it is an approximation to consider that the internal separation $\frac{Q_{sep}}{Q_{\text{in},o}}$ depends only on Q_O, but the other factors (e.g., Q_U) affecting the separation are kept constant. The approximation can be expected to be valid with minor changes to these other factors.

DYNAMIC MASS-BALANCE MODEL

This section gives a mass-balance control-oriented model of a hydrocyclone. The hydrocyclone is divided into two virtual

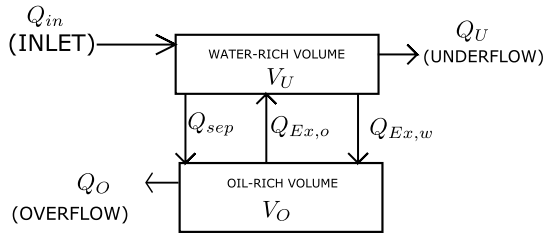

Figure 11. Simplified representation of the model.

control volumes. First, the volume V_O at the center of the hydrocyclone is the "oil-rich volume" related to the overflow. This volume is assumed to have the same shape as the hydrocyclone as shown in Figure 10a. A second volume outside V_O is the "water-rich volume", V_U. Most of the V_U is filled with water as the expected inlet oil fraction is less than 5% of the total inflow rate. The total hydrocyclone volume is V_{HC}, and the water-rich volume is thus given as $V_U = V_{HC} - V_O$. V_O is always wholly within the reverse-flow zone, while V_U is predominantly in the forward-flow direction and partially in the reverse-flow zone. V_O and V_U are time-varying, while $V_{HC} = V_U + V_O$ is a constant.

Figures 10b–d shows how the separation of oil (yellow) and water (blue) depends on the overflow rate. Note that the hydrocyclone liners and the oil core are magnified in Figure 10 for the purpose of demonstration; in reality, they are longer and thinner. Also, the dimensions of underflow and overflow pipe section and the control valves in Figure 10a are bigger than the underflow and overflow outlets of the hydrocyclone liners. The oil droplets entering the reverse-flow zone (marked by the red color in Figure 10a–d) get separated and move toward the oil-rich volume. The droplets that are not separated remain in the water-rich volume and come out with underflow (the thin yellow line in V_U represents oil droplets that are not separated).

In Figure 10b, the overflow radius is large and the oil-rich volume V_O is not completely filled up by oil. Thus, some excess water ($Q_{Ex,\,w}$) flows from V_U to V_O to fill up the remaining space in V_O. During this period, the overflow outlet will have both water and oil. As the overflow decreases, at some point, the entire V_O is filled with oil as shown in Figure 10c. Further reduction forces separated oil into V_U, and we assume that this separated excess oil flows back to V_U (marked with green arrows in Figure 10d). This excess flow of oil ($Q_{Ex,\,o}$) (back-flow) enters the water-rich volume and comes in the underflow. It is assumed that the back-flow of oil never re-enters the oil-rich volume.

For the mass balance analysis, we consider separately the oil and the water inside the two volumes V_O and V_U and get (see Figure 11)

$$\frac{dV_{O,o}}{dt} = Q_{sep} - Q_{O,o} - Q_{Ex,o} \tag{24}$$

$$\frac{dV_{U,o}}{dt} = Q_{\text{in},o} - Q_{sep} - Q_{U,o} + Q_{Ex,o} \tag{25}$$

$$\frac{dV_{O,w}}{dt} = Q_{Ex,w} - Q_{O,w} \tag{26}$$

$$\frac{dV_{U,w}}{dt} = Q_{\text{in},w} - Q_{Ex,w} - Q_{U,w} \tag{27}$$

Here, $V_{O,\,o}$ is the volume of oil in V_O, $V_{U,\,o}$ is the volume of the oil in V_U, $V_{O,\,w}$ is the volume of water in V_O, $V_{U,\,w}$ is the volume of water in V_U, Q_{sep} is the flowrate of the separated oil entering V_O, $Q_{O,\,o}$ is the flowrate of oil at the overflow, $Q_{U,\,o}$ is the flowrate of oil at the underflow, $Q_{in,\,o}$ is the inflow rate of oil, $Q_{Ex,\,o}$ is the excess flow rate of oil (entering into V_U), $Q_{Ex,\,w}$ is the excess flow of water (entering into V_O), $Q_{O,\,w}$ is the flowrate of water at the overflow, $Q_{U,\,w}$ is the flowrate of water at the underflow, and $Q_{in,\,w}$ is the inflow rate of water.

If $\beta_{in,\,o}$ and Q_{in} are the volume fraction of oil in the feed and the total inflow rate (oil and water), respectively, then

$$Q_{\text{in},o} = \beta_{\text{in},o} Q_{\text{in}} \tag{28}$$

$$Q_{\text{in},w} = (1 - \beta_{\text{in},o}) Q_{\text{in}} \tag{29}$$

The internal separated oil is from eq 23

$$Q_{sep} = Q_{\text{in},o}(p_2 Q_O^2 + p_1 Q_O + p_0) \tag{30}$$

where Q_O is the overflow rate. The volume fractions of oil and water in the two volumes V_O and V_U are defined as

$$\beta_{O,o} = \frac{V_{O,o}}{V_O} \tag{31}$$

$$\beta_{O,w} = 1 - \beta_{O,o} \tag{32}$$

$$\beta_{U,o} = \frac{V_{U,o}}{V_U} \tag{33}$$

$$\beta_{U,w} = 1 - \beta_{U,o} \tag{34}$$

The excess oil entering V_U is

$$Q_{Ex,o} = \begin{cases} Q_{sep} - Q_O, & \text{if } Q_{sep} - Q_O > 0 \\ 0, & \text{otherwise} \end{cases} \tag{35}$$

The excess water entering V_O is

$$Q_{Ex,w} = \begin{cases} Q_O - Q_{sep}, & \text{if } Q_{sep} - Q_O < 0 \\ 0, & \text{otherwise} \end{cases} \tag{36}$$

Assuming for simplicity that the internal volumes V_O and V_U are well mixed so that the compositions in the outflows Q_O and Q_U are the same as inside, we get from definitions 31–34:

https://dx.doi.org/10.1021/acs.iecr.0c02859
Ind. Eng. Chem. Res. 2020, 59, 18937–18950

$$Q_{O,o} = \beta_{O,o} Q_O \tag{37}$$

$$Q_{U,o} = \beta_{U,o} Q_U \tag{38}$$

$$Q_{O,w} = \beta_{O,w} Q_O \tag{39}$$

$$Q_{U,w} = \beta_{U,w} Q_U \tag{40}$$

Rewriting eqs 24−27 in terms of volume fractions gives

$$\frac{d\beta_{O,o}}{dt} = \frac{1}{V_O}(Q_{sep} - \beta_{O,o} Q_O - Q_{Ex,o}) \tag{41}$$

$$\frac{d\beta_{U,o}}{dt} = \frac{1}{V_F}(Q_{\text{in},o} - Q_{sep} - \beta_{U,o} Q_U + Q_{Ex,o}) \tag{42}$$

$$\frac{d\beta_{O,w}}{dt} = \frac{1}{V_O}(Q_{Ex,w} - \beta_{O,w} Q_O) \tag{43}$$

$$\frac{d\beta_{U,w}}{dt} = \frac{1}{V_F}(Q_{\text{in},w} - Q_{Ex,w} - \beta_{U,w} Q_U) \tag{44}$$

The two outlet flows are given from eqs 6 and 7. Here, from eqs 31−34, we can also choose the pair 41−42 or the pair 43−44 as model equations.

SUMMARY OF THE MODELS

The model in this paper can be divided into three parts. The first part gives a static relationship between the pressures and the flows using Bernoulli's equations. If we know the inlet pressure and the inlet oil fraction, then the static relationship described in the Pressure-Flow Relationship section (eqs 4−8) gives the two outlet pressures (P_2 and P_3) and the two volumetric outflows (Q_U and Q_O).

The second part of the model is given in the Modeling of Internal Separation section. Here, the separation of oil droplets inside the cyclone liner is determined. A polynomial approximation of the separation as a function of overflow volumetric flow rate for use in the control-oriented model is given in eq 23. The calculation of the separation uses the droplet trajectory analysis described in the Oil Droplet Trajectory Analysis section and the pressure-flow relationship described in the Pressure-Flow Relationship section.

The third part of the model is a control-oriented dynamic mass-balance relationship of the oil fraction inside a hydrocyclone liner, and this is given in the Dynamic Mass-Balance Modelsection, see eqs 41−42. The pressure-flow relationship and the separation are used in the dynamic model for calculating the volumetric flow rate of oil. This dynamic mass-balance relationship gives the fraction of oil and water at the underflow (water) outlet ($\beta_{U,o}$, $\beta_{U,w}$) and the overflow (oil) outlet ($\beta_{O,o}$, $\beta_{O,w}$).

VALIDATION OF MODELS

The different parts of models are here validated against experimental data from the literature.

Validation of Pressure-Flow Relationship. The experimental results from ref.8 shows that the pressure drop from the inlet to the underflow (dP_u) is less than that from the inlet to the overflow (dP_o) and increases as the flow rate increases. Figure 12 shows the experimental result (dP_u(Exp) and dP_o(Exp)) from ref 8 and the simulation results (dP_u(Sim) and dP_o(Sim)) of eqs 4−8 in normalized axes. The simulation is done with boundary condition P_1 = 6 bar. From the plots, it can be seen that the behavior of experimental results and the simulation results is similar.

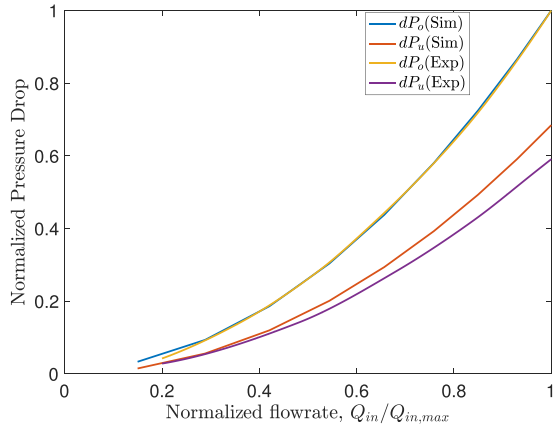

Figure 12. Pressure drop versus flow rate relationship using the experimental results (ref 8) and the simulation results of eqs 4−8.

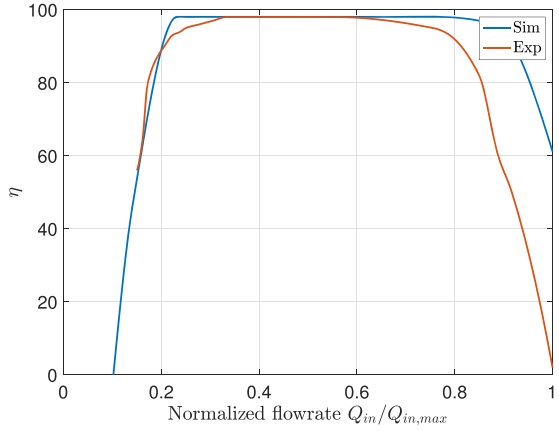

Figure 13. Experimental results (ref 8) and simulation results for efficiency η as a function of Q_{in} of de-oiling hydrocyclone with a constant overflow valve opening.

Validation of Droplet Trajectory Model. The experimental data for the separation efficiency η from ref 8 are shown in Figure 13. The separation efficiency η is defined by eq 2. We use the method described in the Modeling of Internal Separation section and summarized in Figure 8 (i.e., combining the droplet trajectory model and pressure-flow relationship) for calculating the internal separation. Here, the overflow valve is kept constant, the inlet pressure P_1 is set at 6 bar, inlet oil concentration as 1000 ppm, and the droplet distribution as shown in Figure 7. The resulting simulated separation efficiency is also shown in Figure 13. This separation efficiency is calculated using a static model without considering the excess oil flow ($Q_{Ex,o}$). Including this effect would make the efficiency drop more sharply. The separation efficiency increases with flow rate, then it remains constant for certain range of flow rate and then decreases sharply. It can be seen that the simulation results match the behavior of the experimental results.

DYNAMIC SIMULATION OF THE MODEL UNDER CLOSED-LOOP CONTROL

For the dynamic simulation, the underflow valve is kept at a fixed opening of 50%. (This value is not an optimal one; further investigation needs to be done to maximize the underflow rate

https://dx.doi.org/10.1021/acs.iecr.0c02859
Ind. Eng. Chem. Res. 2020, 59, 18937−18950

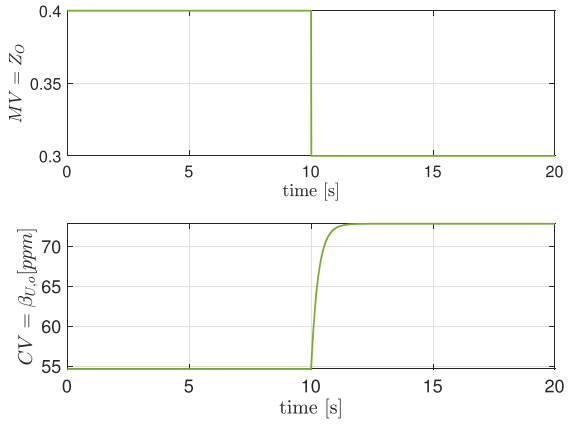

Figure 14. Dynamic effect of MV (Z_O) on the CV ($\beta_{U,o}$).

and keeping the oil fraction at the underflow at a minimum.) The overflow valve is used as the manipulated variable (MV) to control the oil in water ($\beta_{U,o}$) setpoint of 30 ppm (we assume that 30 ppm ≈ 30 mg/L). We assume that we can measure the oil-in- water concentration $\beta_{U,o}$ online (e.g., ref 19). Also, the results from ref 20 are promising in terms of using the oil-in-water sensor for control purposes.

Figure 14 shows the dynamic effect of a step change in the MV (Z_O) on the CV ($\beta_{U,o}$). This shows a first-order response with the process gain $k = -1.82 \times 10^{-4}$, process time constant τ_1 = 0.28 s, and time delay τ_d = 0.002 s. If we choose the closed-loop response time τ_c = 1.5 s, then, based on SIMC rules,[21] we have the proportional-integral (PI) controller of the form $K_c\left(1 + \frac{1}{\tau_I s}\right)$, where $K_c = -1012$ and $\tau_I = -0.285$ s.

There are no experimental results to validate the dynamic model in the literature because most of the available data is based on pressure difference ratio (PDR) control and not giving the outlet purity $\beta_{U,o}$. Figure 15 shows the block diagram representation of the plant model and the controller used for the simulations. Values of different parameters used in the simulation are listed in Table 1 (we have considered a Colman and Thew's type hydrocyclone liner[11,22]), and the tuning factors used in the simulation are given in Table 2. Here, we take inlet pressure P_1 = 6 bar as the boundary condition.

Table 2. Values of Tuning Factors Used in the Model

tuning factor	value
α	0.175
α_2	2.67
n	0.63
$R_{fac,1}$	0.3714
$R_{fac,2}$	0.27

The proposed controller is tested in closed-loop simulations in seven plausible scenarios as shown in Figures 16−. The simulation results are also summarized in Table 3. Note that, in scenarios 1−6, all cases are operating with excess water in the oil overflow as shown in Figure 10b. Scenario 7 operates with excess oil flow to V_U. The results are discussed next.

For Scenario 1, we have an increase in the inlet oil concentration $\beta_{in,o}$ from 1000 to 1200 ppm. To separate this additional oil, the centrifugal force has to be increased. An increase in the inflow rate Q_{in} increases the centrifugal force and hence the separation. To increase Q_{in}, we have to increase Q_O (the underflow valve opening Z_U is fixed in the simulation). Indeed, the controller opens the overflow valve and the overflow rate increases; thus, the purity of the underflow outlet is maintained at 30 ppm.

A decrease in the inlet oil concentration (Scenario 2) naturally causes a decrease in the oil concentration in the underflow. The controller reduces the overflow opening to maintain the 30 ppm setpoint.

For Scenario 3, an increase in the underflow valve opening causes a sudden decrease in the overflow rate, which makes the separation less efficient. The controller opens the overflow valve to maintain the 30 ppm setpoint.

In the case where the underflow valve opening is decreased, the underflow rate decreases and causes a sudden increase in the overflow rate (Scenario 4). This improves separation; however, the controller reduces the overflow opening to maintain the 30 ppm setpoint.

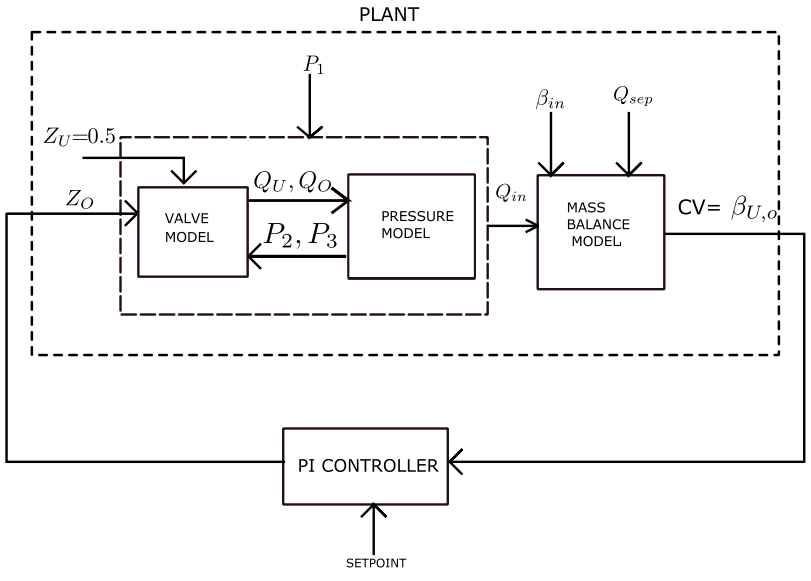

Figure 15. Control structure.

https://dx.doi.org/10.1021/acs.iecr.0c02859
Ind. Eng. Chem. Res. 2020, 59, 18937−18950

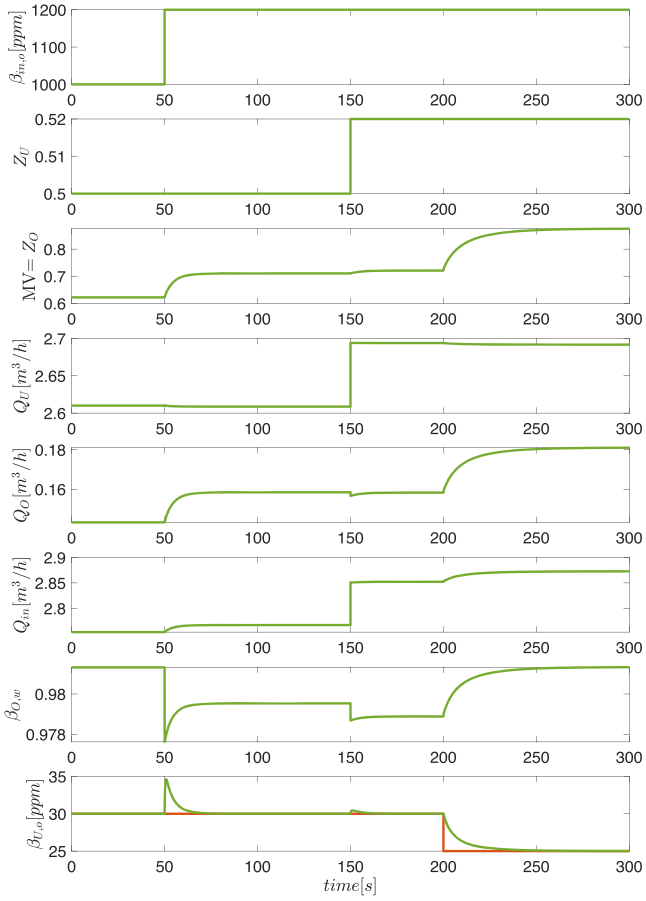

Figure 16. Simulation of control system in Figure 15 for Scenarios 1, 3, and 5; an increase in inlet oil fraction at t = 50, increase in underflow rate at t = 150, and decrease in setpoint at t = 200.

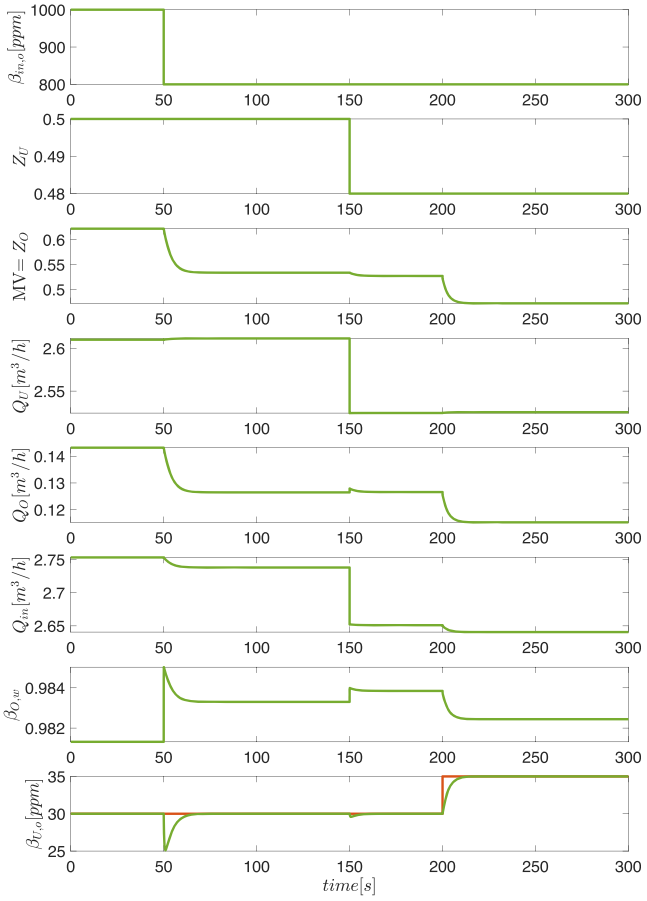

Figure 17. Simulation of control system in Figure 15 for Scenarios 2, 4, and 6 ; a decrease in inlet oil fraction at t = 50, decrease in underflow rate at t = 150, and increase in setpoint at t = 200.

Finally, Scenarios 5 and 6 consider the closed-loop response to a setpoint change. The controller tracks the setpoint change with a response time of 5 s.

In the above simulations, we have no oil back flow ($Q_{Ex,\,o} = 0$). Hence, to test the effect of excess oil flow to V_U, we start the simulation with a setpoint of 100 ppm and later at t = 50 increase the setpoint to 200 ppm. Figure 18 shows the simulation result of this scenario (Scenario 7). Here, the controller closes the overflow valve to attain the setpoint. Due to the small overflow opening, the excess oil flow back to V_U as demonstrated in Figure 10d and the fraction of water $\beta_{O,\,w}$ at the overflow becomes zero.

For Scenario 8, we do an open-loop simulation with the overflow valve at 12% opening and the underflow valve at 50% opening. The inlet oil concentration is increased from 1600 to 15,000 ppm at t = 50. Due to the increase in the inlet oil concentration, more oil flows in to V_O and fraction of water ($\beta_{O,\,w}$) becomes zero. The overflow opening is not large enough to take excess oil. Hence, the oil flow backs to V_U and $Q_{Ex,\,o} > 0$. Figure 19 shows the simulation result of this scenario (Scenario 8).

An industrial control system controls the pressure drop ratio (PDR) to maintain the efficiency of the hydrocyclones. PDR control is an indirect way of achieving the specified criteria. If there is an increase in the inlet oil concentration, then it is required to manually change the setpoint of the PDR controller to maintain the efficiency.[8] One of the future works to improve the PDR control strategy is to adjust the PDR setpoint in a cascade manner. More specifically, we propose to use the oil fraction $\beta_{U,\,o}$ (at the underflow water outlet) as the controlled variable (CV) and the PDR setpoint as the manipulated variable (MV).

CONCLUSIONS

A first-principles control-oriented model was developed for a de-oiling hydrocyclone. The development of the model was divided into three main parts: first, a droplet trajectory analysis for calculating the separation; second, a static pressure-flow model; and third, a dynamic mass-balance model. Combining these different gives a dynamic model, which is suitable for process control. In this paper, the proposed model uses the simplified polynomial approximation of the separation. The static models for pressure-flow relationship and the separation efficiency were qualitatively validated against the experimental results from the literature.

A PI controller was implemented to test the derived dynamic model. The simulation results show that the model gives the expected behavior for different scenarios. The goal of the controller was to keep a constant setpoint of 30 ppm oil for $\beta_{U,\,o}$ varying the overflow valve opening.

As a future work, the dynamic model is planned to be validated using experiments in a newly constructed laboratory. The model developed is non-linear in nature, giving opportunities for developing advanced non-linear control algorithms. Another future investigation is to optimize the number of hydrocyclone liners (here we have considered a single liner).

https://dx.doi.org/10.1021/acs.iecr.0c02859
Ind. Eng. Chem. Res. 2020, 59, 18937−18950

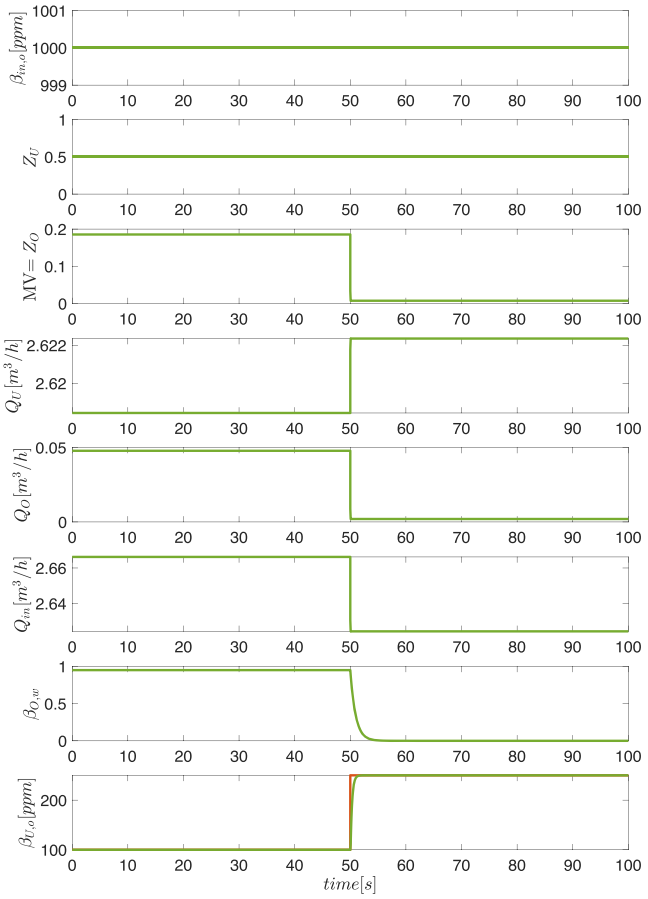

Figure 18. Simulation of Scenario 7; an increase in setpoint from 100 to 200 ppm at t = 50 causing excess oil flow $Q_{Ex,\,o}$ to V_U.

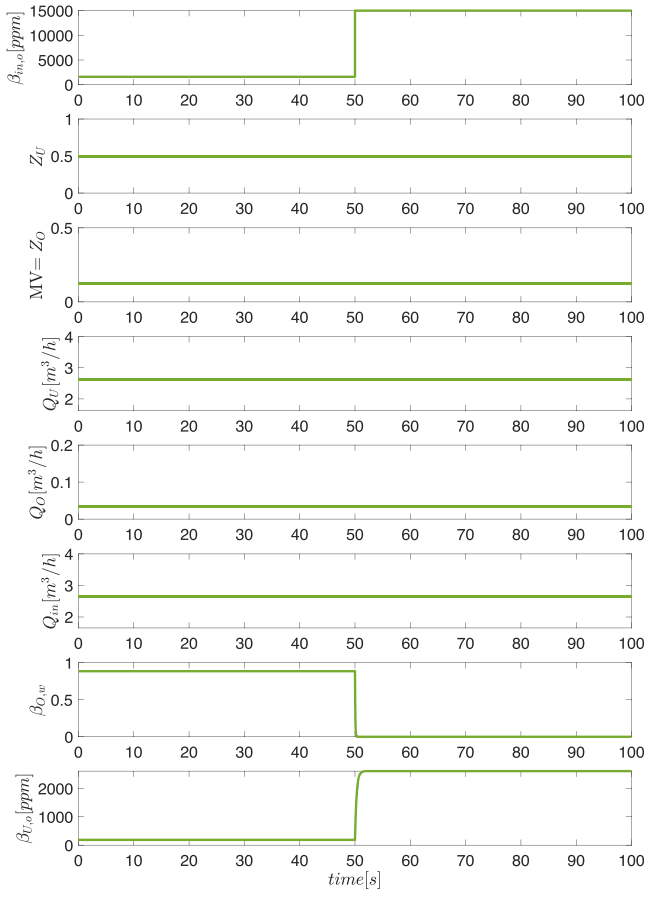

Figure 19. Simulation of Scenario 8; an open-loop simulation where the overflow valve opening is fixed at 12% and the underflow valve opening is fixed at 50% and at t = 50, $\beta_{in,\,o}$ is increased from 1600 to 15,000 ppm causing excess oil flow $Q_{Ex,\,o}$ to V_U.

APPENDIX A: TANGENTIAL KINETIC ENERGY AT THE UNDERFLOW

This appendix gives the derivation of the tangential kinetic energy ($KE_{U\theta}$) at the underflow outlet of a hydrocyclone liner. It is assumed that reverse-flow zone extends to the underflow so that the tangential velocity profile at the underflow will have a Rankine vortex profile as shown in Figure 2. Substituting $R(z) = R_U$ in Figure 2 gives the tangential profile representation at the underflow outlet.

The tangential velocity V_{t1} (shown in Figure 2) of the fluid at the free vortex part is

$$V_{t1} = \frac{a_1}{r} \tag{45}$$

Table 3. Discussion of Simulation Results in Figures 16−19

#	description	behavior of the controller
1	Increase in inlet oil concentration (from 1000 to 1200 ppm).	The controller opens up the overflow control valve and the overflow rate Q_O increases.
2	Decrease in inlet oil concentration (from 1000 to 800 ppm).	Due to the criteria of 30 ppm as a setpoint, the controller reduces the overflow rate to achieve the setpoint.
3	Increase in underflow rate by opening the underflow valve from 50% to 52%.	The controller opens the overflow valve, which increases the overflow rate, which in turn reduces the underflow rate.
4	Decrease in underflow rate by closing the underflow valve from 50% to 48%.	Controller closes the overflow valve to attain the setpoint, though the reduction in ppm at the underflow is a desired scenario.
5	Decrease in setpoint (from 30 to 25 ppm).	The controller tracks the setpoint change with a response time of 5 s.
6	Increase in setpoint (from 30 to 35 ppm).	The controller tracks the setpoint change with a response time of 5 s.
7	A change in setpoint from 100 to 200 ppm to test the excess oil flow to V_U.	To achieve the setpoint of 200 ppm overflow valve closes, the small opening of overflow outlet causes backflow of oil to V_U and $\beta_{O,\,w}$ becomes zero.
8	A change in inlet oil fraction from 1600 to 15,000 ppm to test the excess oil flow to V_U.	The simulation is done in open loop with overflow control valve at 12% opening and underflow control valve at 50% opening. As the overflow opening is not large enough to take out the increase of oil due to change in the inlet oil concentration, the excess oil flows back to V_U, making $Q_{Ex,\,o} > 0$.

https://dx.doi.org/10.1021/acs.iecr.0c02859
Ind. Eng. Chem. Res. 2020, 59, 18937−18950

The tangential velocity V_{t2} (shown in Figure 2) of the fluid at the forced vortex part is

$$V_{t2} = a_2 r \tag{46}$$

Here, r represents the radial distance of the vortex from the center, and a_1 and a_2 are proportionality constants. The computation of constant a_1 can be done using eq 9 where n = 1 and also taking the inlet velocity v_{in} and the radius of the first cylindrical part of the cyclone R_1 as

$$a_1 = \alpha_1 \frac{Q_{in} R_1}{\pi R_{in}^2} \tag{47}$$

Peak tangential velocity occurs at the boundary of the reverse-flow zone as shown in Figure 2, and V_{t1} and V_{t2} are equal at $R_{U,\,rev} = R_{fac,2} R_U$:

$$a_2 R_{U,rev} = \frac{a_1}{R_{U,rev}} \rightarrow a_2 = \frac{a_1}{R_{U,rev}^2} \tag{48}$$

Then, the average kinetic energy contributed by the tangential velocity is given as

$$\begin{aligned} KE_{U\theta} &= \frac{\rho_U}{2}\frac{1}{A_U}\left[\int_0^{2\pi}\int_{R_{U,rev}}^{R_U}\left(\frac{a_1}{r}\right)^2 dA + \int_0^{2\pi}\int_0^{R_{U,rev}}(a_2 r)^2 dA\right] \\ &= \frac{\rho_U}{2}\frac{2}{R_U^2}\left[\int_{R_{U,rev}}^{R_U}\left(\frac{a_1}{r}\right)^2 r dr + \int_0^{R_{U,rev}}(a_2 r)^2 r dr\right] \\ &= \frac{\rho_U}{2}\frac{2}{R_U^2}\left[a_1^2(\ln(R_U) - \ln(R_{U,rev})) + \frac{a_2^2}{4}R_{U,rev}^4\right] \\ &= \frac{\rho_U}{2}\frac{2}{R_U^2}\left[a_1^2(\ln(R_U) - \ln(R_U R_{fac,2})) + \frac{a_2^2}{4}R_{U,rev}^4\right] \end{aligned}$$

The difference $\ln(R_U) - \ln(R_U R_{fac,2}) \in [0.9,1.3]$ (approximated as 1) when the $R_{fac,2} \in [0.27,0.4]$. Hence

$$KE_{U\theta} = \frac{5}{4}\frac{\rho_U}{R_U^2}\frac{(\alpha_1 Q_{in} R_1)^2}{\pi^2 R_{in}^4}$$

APPENDIX B: TANGENTIAL KINETIC ENERGY AT THE OVERFLOW

This appendix gives the derivation of the tangential kinetic energy ($KE_{O\theta}$) at the overflow outlet of a hydrocyclone liner. The tangential velocity at the overflow has only the forced vortex part of the Rankine vortex and hence tangential velocity is given by eq 46. Then, the average kinetic energy contributed by this tangential velocity is given as

$$\begin{aligned} KE_{O\theta} &= \frac{\rho_O}{2}\frac{1}{A_O}\left[\int_0^{2\pi}\int_0^{R_O}(a_2 r)^2 dA\right] \\ &= \frac{\rho_O}{R_O^2}\left[\int_0^{R_O}(a_2 r)^2 r dr\right] = \frac{\rho_O}{R_O^2}\left[\int_0^{R_O}\left(\frac{a_1}{R_{U,rev}^2}\right)^2 r^3 dr\right] \\ &= \frac{\rho_O}{4}\frac{(\alpha_1 Q_{in} R_1)^2}{(\pi R_{in}^2)^2 R_{U,rev}^4} R_O^2 \end{aligned}$$

AUTHOR INFORMATION

Corresponding Authors

Mishiga Vallabhan K G − *Department of Mechanical and Industrial Engineering, NTNU Norwegian University of Science and Technology, Trondheim 7491, Norway*; orcid.org/0000-0002-5722-0851; Email: mishiga.vallabhan@ntnu.no

Christian Holden − *Department of Mechanical and Industrial Engineering, NTNU Norwegian University of Science and Technology, Trondheim 7491, Norway*; Email: christian.holden@ntnu.no

Sigurd Skogestad − *Department of Chemical Engineering, NTNU Norwegian University of Science and Technology, Trondheim 7481, Norway*; Email: sigurd.skogestad@ntnu.no

Complete contact information is available at: https://pubs.acs.org/10.1021/acs.iecr.0c02859

Notes

The authors declare no competing financial interest.

ACKNOWLEDGMENTS

This project is supported by the Norwegian Research Council, industrial partners, and NTNU under the Subsea Production and Processing (SUBPRO) SFI program.

REFERENCES

(1) OSPAR *Discharges, OSPAR convention*; 2001https://www.ospar.org/work-areas/oic/discharges, (accessed Sep 23, 2020).

(2) Georgie, W. J. *Effective and Holistic Approach to produced Water Management for Offshore Operation*; Offshore Technology Conference: Houston, Texas, 2002; 13.

(3) Orlowski, R.; Euphemio, M. L. L.; Euphemio, M. L.; Andrade, C. A.; Guedes, F.; da Silva, L. C. T.; Pestana, R. G.; de Cerqueira, G.; Lourenço, I.; Pivari, A.; Witka, A.; Folhadella, H.; Pacheco, L.; Kronemberger, S.; Vilela, J. *Marlim 3 Phase Subsea Separation System - Challenges and Solutions for the Subsea Separation Station to Cope with Process Requirements*; Offshore Technology Conference: Houston, Texas, USA, 2012; 11.

(4) Pereira, R. M.; de Campos, M. C. M. M.; de Oliveira, D. A.; de Souza, R. d. S. A.; Filho, M. M. C.; Orlowski, R.; Duarte, D. G.; Raposo, G. M.; Lillebrekke, C.; Ljungquist, D.; Carvalho, A.; Fares, M. *SS: Marlim 3 Phase Subsea Separation System: Controls Design Incorporating Dynamic Simulation Work*; Offshore Technology Conference: Houston, Texas, USA, 2012; 13.

(5) Svarovsky, L.; Thew, M. *Hydrocyclones: analysis and applications*; Springer Science & Business Media: 2013; *12*.

(6) Colman, D.; Thew, M.; Corney, D. Hydrocyclones for oil/water separation. In *Int. Conf. on Hydrocyclones*; 1980; 143−165.

(7) Thew, M. Hydrocyclone redesign for liquid-liquid separation. *Chem. Eng. (London)* **1986**, 17−23.

(8) Meldrum, N. Hydrocyclones: A Solution to Produced-Water Treatment. *SPE Prod. Eng.* **1988**, *3*, 669−676.

(9) Thew, M. *Encyclopedia of Separation Science*; Elsevier: 20004; 1480−1490.

(10) Das, T.; Jäschke, J. Modeling and control of an inline deoiling hydrocyclone. In *3rd IFAC Workshop on Automatic Control in Offshore Oil and Gas Production OOGP*; 2018, *51*, 138−143.

(11) Wolbert, D.; Ma, B.-F.; Aurelle, Y.; Seureau, J. Efficiency estimation of liquid-liquid Hydrocyclones using trajectory analysis. *AIChE J.* **1995**, *41*, 1395−1402.

(12) Caldentey, J.; Gomez, C.; Wang, S.; Gomez, L.; Mohan, R.; Shoham, O. Oil/water separation in liquid/liquid hydrocyclones (LLHC): Part 2-Mechanistic modeling. *SPE J.* **2002**, *7*, 362−372.

(13) Motin, A. Theoretical and numerical study of swirling flow separation devices for oilwater mixtures. Ph.D. thesis, Michigan State University, 2015.

(14) Kharoua, N.; Khezzar, L.; Nemouchi, Z. CFD Simulation of Liquid-Liquid Hydrocyclone: Oil/Water Application. In *Fluids Engineering Division Summer Meeting*; 2009; 2085−2094.
(15) Durdevic, P.; Pedersen, S.; Bram, M.; Hansen, D.; Hassan, A.; Yang, Z. Control oriented modeling of a de-oiling hydrocyclone. In *17th IFAC Symposium on System Identification SYSID* 2015; *48*, 291−296.
(16) Bram, M. V.; Hansen, L.; Hansen, D. S.; Yang, Z. Hydrocyclone Separation Efficiency Modeled by Flow Resistances and Droplet Trajectories. In *3rd IFAC Workshop on Automatic Control in Offshore Oil and Gas Production*; 2018, *51*, 132−137.
(17) White, F. *Fluid Mechanics; McGraw-Hill series in mechanical engineering*; McGrawHill: 2011; *4*, 283.
(18) Young, G. A. B.; Wakley, W. D.; Taggart, D. L.; Andrews, S. L.; Worrell, J. R. Oil-water separation using hydrocyclones: An experimental search for optimum dimensions. *J. Pet. Sci. Eng.* **1994**, *11*, 37−50.
(19) Mirmorax *Oil-in-water analyzer*; https://mirmorax.com/oil-in-water-analyzer/, (accessed Sep 23, 2020).
(20) Durdevic, P.; Raju, C.; Bram, M.; Hansen, D.; Yang, Z. Dynamic Oil-in-Water Concentration Acquisition on a Pilot-Scaled Offshore Water-Oil Separation Facility. *Sensors* **2017**, *17*, 124.
(21) Skogestad, S. Simple analytic rules for model reduction and PID controller tuning. *J. Process Control* **2003**, *13*, 291−309.
(22) Gomez, C.; Caldentey, J.; Wang, S.; Gomez, L.; Mohan, R.; Shoham, O. Oil/water separation in liquid/liquid hydrocyclones (LLHC): Part 1-Experimental investigation. *Spe J.* **2002**, *7*, 353−372.

https://dx.doi.org/10.1021/acs.iecr.0c02859
Ind. Eng. Chem. Res. 2020, 59, 18937−18950